



Reconstructing human push recovery reactions using a three dimensional under-actuated bipedal robot

Behnam Miripour Fard^a, Ahmad Bagheri^b, Nader Nariman-zadeh^b

^a Department of Robotics Engineering, Hamedan University of Technology, Hamedan, Iran, E-mail: bmf@hut.ac.ir

^b Department of Mechanical Engineering, the University of Guilan, Rasht, Iran, bagheri@guilan.ac.ir, nnzadeh@guilan.ac.ir

ARTICLE INFO

ABSTRACT

Article history:

Received: June 11, 2016

Received in revised form: April 7, 2017

Accepted: June 7, 2017

Keywords:

Inverse biomimetic
biped robot
3D Model
under-actuation
walking push recovery
hybrid feedback control

This paper presents the ability of hybrid zero dynamics (HZD) feedback control method to reproduce human like movements for walking push recovery of an under-actuated 3D biped model. The balance recovery controller is implemented on a three-dimensional under-actuated bipedal model subjected to a push disturbance. The biped robot model is considered as a hybrid system with eight degrees of freedom (DOF) in the single support phase and two degrees of under-actuation in the ankle joint. The control is done based on the method of virtual constraints and HZD, by adjusting the desired trajectory of the event-based feedback controller. Several simulations have been done considering pushes exerted during walking. The results showed the performance of the method in recovery of pushes occurring in the sagittal and frontal planes and also in the both directions, simultaneously. The results showed that the simulated motions can be characterized in terms of strategies observed in human for balance recovery against perturbations during walking.

1. Introduction

Inverse biomimetic has attracted increasing research attention as an interesting approach. This approach starts from the available engineering techniques and computational facilities to explain generation of human or animal behavior [1-2]. This

paper presents an attempt to use the inverse biomimetic approach using a 3D bipedal model to explain human reactions under pushing disturbances during walking. The results of current paper and relevant studies by other researchers from biology and robotics (e.g. references [3-6]) may provide opportunities for joint research projects involving neurobiologists and roboticists.

Biped robots are designed and fabricated to work in environments designed for human. During walking, many perturbations (e. g. stumbling, slipping and pushing) may occur and bipeds should adopt proper responses to avoid falling. Push recovery refers to maintaining biped balance when subjected to a push disturbance. Consideration of spatial and under-actuated models makes it very challenging to study motion planning and control of biped robots when pushed. The objective of the present paper is to address this problem. Control of under-actuated walking is an attractive area of research because the motions achievable by these kinds of bipeds are highly efficient and natural looking in comparison with fully actuated bipeds.

Previous studies on the modeling and control of push can be classified into two categories: Push recovery during standing and push recovery during walking. Upright standing push recovery [7-10] is beyond the scope of this paper and it is totally different from walking push recovery. So, we will briefly review the studies have been done in robotics on the push recovery of walking.

Very few researchers have explored push recovery during walking and there is still a lack of tools for systematic control design and stability analysis, especially for non-periodic motions. Some researchers have focused on the control of fully actuated ZMP based walkers [11-12]. In this approach, a desired trajectory of the ZMP is first defined and a joint or force controller is then applied on the basis of the desired ZMP trajectory. Adiwahono, et al. [13] have proposed some definitions of the types of pushes that may occur during walking, and presented a push recovery algorithm based on the modification of the ZMP reference of the preview controller. Adiwahono, et al. [14-15] also proposed an overall real-time control system and a real-time push recovery controller for humanoid robots with a focus on how to modify the different phases in walking such that the stability can be maintained. Their proposed real-time push recovery controller uses body linear velocity, body inclination, and ground reaction force as a feedback to modify the gait. Urata et al. [16] have introduced an online decision method of foot placement using a fast trajectory generation method that manages pushes. Wang et al. [17] have studied the push recovery for a 3D biped robot with flat-feet based on the control of the ZMP, the swing ankle rotation and the partial joints angles simultaneously. However, there are still a few researches on the push recovery of under-actuated walkers (limit cycle walkers), whereas the motions achievable by them are energy efficient and natural.

See ref. [18] and references therein for a review of push recovery studies of limit cycle walkers.

Most of the above mentioned studies have been done in the plane. One important reason is that in 3D case, dynamics of the robot becomes more complex with several highly coupled degrees of freedom. Furthermore, the degree of under-actuation for 3D bipeds with point-feet contact is two or more than two (in the single support phase); therefore it would be hard to control them under external disturbances. Under-actuated walkers with point-feet contacts have generated much interest for researchers because they show highly efficient and natural motions [18]. To the best of current author's knowledge, although there is no work on the push recovery of under-actuated spatial bipeds with point-feet contact in the open literature but there are some valuable studies on the feedback control of these robots during normal walking and running. One of the important works has done by Chevallereau et al. [19] in which a time-invariant feedback control law has been developed for a 3D bipedal model that induces asymptotically stable walking. They used the method of virtual constraints and hybrid zero dynamics (HZD) in order to produce an autonomous feedback controller that realizes the stable periodical orbit for the model. They also extended the work to study steering of the model using an event-based feedback controller in order to achieve a desired amount of turning [20]. Song and Zefran [21] have designed a controller for a five-link 3D robot with un-actuated point-feet on the basis of linearizing the robot's dynamic model along a periodic orbit.

In the present study, a 3D hybrid nonlinear under-actuated biped model with eight degrees of freedom and six actuators is considered which experiences a pushing force during walking. An event-based hybrid feedback controller has been implemented to recover orbital stability of the robot after push. This is accomplished by adjusting the desired trajectory of controller. The range of perturbation forces which the method can reject in each direction to continue cyclic walking has been obtained. The contribution of this work is that the simulated movements have been characterized based on human observed strategies for balance recovery. The overall stability of walking, that is the convergence to a periodic walking after push, was shown through simulation.

In the following section, the model of the biped is described and its dynamic equations are derived. The control strategy is detailed next and then the simulation results are discussed. Finally, concluding remarks are drawn.

2. Dynamical model of the bipedal robot

The studied three-dimensional bipedal model consists of five rigid segments representing; a torso, two thighs and two shanks (Figure 1). These segments are connected by two hip joints (2 DOF for each hip joint) and two knee joints (1 DOF for each knee joint). The stance leg is assumed to act as a passive pivot in the sagittal and frontal planes, with no yaw rotation (about the x-axis). So, the leg end is modeled as a point contact with 2 DOF. There is no torque at the contact point of the legs with the ground. All actuated joints are assumed as frictionless hinges that are independently actuated. In all the simulations it is assumed that the friction between the point-feet and the ground is sufficient to prevent sliding and yaw rotation. In total, the biped model in the single support phase has 8 DOF and there are two degrees of under-actuation at stance leg contact.

It is assumed that the walking surface is rigid and flat and the transition from one leg to another leg (double support) takes place in an infinitesimal length of time. This assumption entails the use of a rigid model to describe the impact of the swing leg with the ground. The dynamic model of the biped robot thus consists of two parts:

- Dynamics of the robot during the swing phase (single support phase),
- Dynamics of contact events (foot with ground).

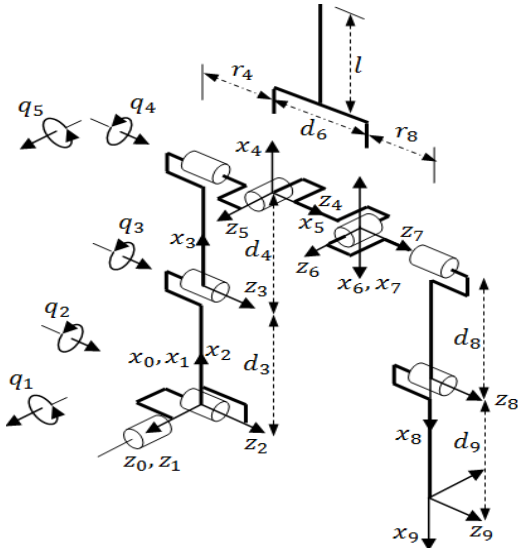


Fig. 1. Model of 3D point-foot biped robot

2.1 Dynamics of the robot in single support phase

During the single support phase of the motion, the stance leg is acting as a 2 DOF pivot, and there are only

8 DOF ($[q_1, q_2, q_3, q_4, q_5, q_6, q_7, q_8]$). In this phase, the biped is equivalent to an open chained manipulator robot. There are two conventional approaches to obtain the equations of the motion of an open chained manipulator consisting of rigid bodies; Newton-Euler (NE) and Euler-Lagrange (EL). For the models with high degrees of freedom the EL method requires complex calculations for partial derivations and the NE formalism is more efficient due to its recursive nature [22]. Using NE recursive formulation [23], the mathematical model describing the biped motion in the swing phase is obtained. The objective is to represent the equations for the single support phase in the following form

$$M(q)\ddot{q} + N(q, \dot{q})\dot{q} + G(q) = Su \quad (1)$$

and to obtain matrices $M(q)$, $N(q, \dot{q})$ and $G(q)$. In the Eq. (1) q is vector of generalized coordinates depicted in Figure 1, the set (q, \dot{q}) constitutes the state of the biped, $M(q) \in \mathbb{R}^{8 \times 8}$ is the mass-inertia matrix, $N(q, \dot{q}) \in \mathbb{R}^8$ contains the centrifugal and Coriolis forces terms, $G(q) \in \mathbb{R}^8$ is the vector of gravitational forces, $u = [u_3, u_4, u_5, u_6, u_7, u_8]^T$ is the vector of control inputs and $S \in \mathbb{R}^{8 \times 6}$ is a torque distribution matrix. Similar to [24] and based on [25] a modified Denavit-Hartenberg (DH) notation is used for geometric description of the biped model. For more details about geometric description and NE recursive method for the above mentioned model, see Appendix A.

It should be mentioned that the equations are solved using a commercial software package (MATLAB release 2014a, The MathWorks, Inc., Natick, MA, USA) and the outputs which are the matrixes in Eq. (1) are written as functions for future uses.

2.2 Dynamic equations of contact events

The end of the single support phase is characterized by a collision between the swing foot and the ground. The impact between the swing leg end and the ground is modeled as an instantaneous inelastic contact between two rigid bodies. The basic assumptions for impact are

- the impact takes place over an infinitesimally small period of time;
- the model walks on a normal ground that is not slippery and sticky. The contact of the swing leg with the ground is assumed to be perfectly inelastic;

- (iii). the external forces during the impact can be represented by impulses;
- (iv). impulsive forces may result in an instantaneous change in the velocities of the generalized coordinates, but the positions remain continuous;
- (v). the torque supplied by the actuators is not impulsive.

The contact model requires the full 14 DOF of the robot. The position of the robot in the double support is defined by $q_e = [q, r_0, \alpha_0]^T \in \mathbb{R}^{14}$ where $r_0 = [x_0, y_0, z_0]$ are the Cartesian coordinates of the stance foot and α_0 defines the rotation along the x-axis of the stance leg. The velocity of the robot and the acceleration are defined by $\dot{q}_e = [\dot{q}, \dot{r}_0, \dot{\alpha}_0]^T \in \mathbb{R}^{14}$ and $\ddot{q}_e = [\ddot{q}, \ddot{r}_0, \ddot{\alpha}_0]^T \in \mathbb{R}^{14}$ respectively. The dynamic equation of the model in double support is represented as

$$M_e(q_e)\ddot{q}_e + N_e(\dot{q}_e, q_e) + G_e(q_e) + D_8 GRF_9 \quad (2)$$

$$= D_u u + D_0 GRF_0$$

where $M_e \in \mathbb{R}^{14 \times 14}$ is the symmetric definite positive inertia matrix, $N_e \in \mathbb{R}^{14}$ represents the Coriolis and centrifugal forces, $G_e \in \mathbb{R}^{14}$ is the vector of gravity. $GRF_0 = [{}^0f_0, {}^0n_0]^T$ is the vector of the ground reaction forces and torques on the stance foot (there are no torques in this study), $GRF_9 = [{}^9f_9, {}^9n_9]^T$ represents the vector of forces exerted by the swing foot on the ground, D_8 , D_u and D_0 are matrices that allow to take into account the forces and torques in the dynamic model. The model of impact which can be deduced from integration of (2) in infinitesimal time and is

$$M_e(q_e) (\dot{q}_e^+ - \dot{q}_e^-) + D_8 I_9 = D_0 I_0 \quad (3)$$

where I_9 and I_0 are the intensity of Dirac delta-function for the forces GRF_9 and GRF_0 , respectively. \dot{q}_e^+ is the velocity just after the impact and \dot{q}_e^- is the velocity just before the impact. Since the stance leg is assumed to detach from the ground without interaction, the external forces acting at the pivot point are zero ($I_0 = 0_{6 \times 1}$). Thus, the impact dynamic model is

$$M_e(q_e) (\dot{q}_e^+ - \dot{q}_e^-) = -D_8 I_9 \quad (4)$$

Additional equations can be obtained from the condition that the impacted leg does not rebound nor slips at impact, which is

$$D_8^T \dot{q}_e^+ = 0_{6 \times 1} \quad (5)$$

$${}^0 \begin{bmatrix} \dot{q}_e^- \\ \omega_0^- \end{bmatrix} = \begin{bmatrix} 0_{3 \times 1} \\ 0_{3 \times 1} \end{bmatrix} \quad (6)$$

Eq. (4), (5) and (6) are linear in the unknowns and determine the impulse forces I_9 and the velocity vector of the biped after impact \dot{q}_e^+

$$I_9 = (D_8^T M_e^{-1} D_8)^{-1} D_8^T \dot{q}_e^- \quad (7)$$

$$\dot{q}_e^+ = -M_e^{-1} D_8 (D_8^T M_e^{-1} D_8)^{-1} D_8^T \dot{q}_e^- + \dot{q}_e^- \quad (8)$$

Eq. (8) is an expression for \dot{q}_e^+ in term of \dot{q}_e^- , which should then be used to re-initialize the model (Eq. (1)). So, a change of coordinates is necessary since after impact with ground the swing leg becomes the new stance leg and vice versa. This is done by computation of the orientation and the angular velocity of the swing leg shank. From this, q_0 , q_1 , and q_2 in the new coordinate can be obtained that are compatible with this orientation. \dot{q}_0 , \dot{q}_1 and \dot{q}_2 are then obtained in similar way. The angles q_3 to q_8 exchange their roles as: $[q_3, q_4, q_5, q_6, q_7, q_8] \rightarrow [q_8, q_7, q_6, q_5, q_4, q_3]$.

To summarize, the global impact model that includes both the jumps in velocities and the swapping of coordinates and velocities can be shortly written as:

$$\begin{pmatrix} q_e^+ \\ \dot{q}_e^+ \end{pmatrix} = \Delta(q_e) \begin{pmatrix} q_e^- \\ \dot{q}_e^- \end{pmatrix} \quad (9)$$

where Δ represents the global mapping matrix.

2. 3 dynamic equations considering push

The push can be happen in single support and or in double support phase of walking. It also can be considered as a force applied for an infinitesimal period of time (impulse) or a force applied for a finite duration of time. For the push occurring in the double support, 14 DOF of the model should be included in the modeling, whereas for the single support phase only 8DOF is sufficient. If the push is impulsive, impact dynamic equations of the model can be derived by applying the principles of linear and angular impulse and momentum. As an example of impulse and impulse moment equations derivation after impulsive push see ref. (18). In this paper, the push is considered as a force applied in finite time duration during the single support phase. Consideration of pushing force in the single support phase seems reasonable because the double support phase was considered to be instantaneous. However, even if the push occurs in the single support phase; its effect on the states of the model will be

appeared in the impact model of the subsequent double support. The method for relating the states of the system before impact and after impact obtained in the previous sub section is used.

The free-body diagram of the model showing pushing forces is shown in Figure 2. P_y and P_z are the components of pushing force applied on the hip joints.

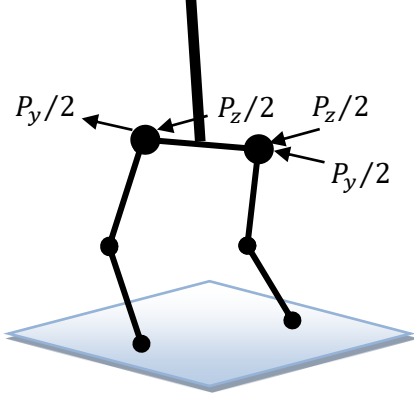


Fig. 2. Free body diagram showing push forces applied on hip joints

To solve the equations of motion in the presence of pushing forces it is sufficient to rewrite the Eq. A.8 (see the appendix) in inward iteration as follow

$${}^j f_j = {}^j R_{j+1} {}^{j+1} f_{j+1} + {}^j F_j + P_j$$

$$P_j = \begin{cases} [0 & P_y/2 & P_z/2]^T & \text{if } j = 4, 7 \text{ and } P_j \\ \equiv 0 & \text{if } j \neq 4, 7. \end{cases} \quad (10)$$

2. 4 Overall model: hybrid system

The overall biped model can now be expressed as a hybrid system with impulse effects. Assuming, $x = [q_e, \dot{q}_e]^T$ and $u = [u_3, u_4, u_5, u_6, u_7, u_8]^T$, in the state space representation the model can be represented as

$$\begin{cases} (1) \text{ Continuous } \{\dot{x}(t) = f(x(t)) + g(x(t))u(t), & \} \\ (2) \text{ Impact model } \{x^+(t) = \Delta x^-(t), & x^-(t) \in S \} \end{cases} \quad (11)$$

where S is switching surface. Contact with the ground is detected when the height of the swing leg is zero

$$S = \{(q, \dot{q}) | x_{\text{swing}} = 0 \text{ and } z_{\text{swing}} > 0\} \quad (12)$$

3. Control strategy

The eight independent degrees of freedom of the model during single support phase can be subdivided into two parts:

$$q_u = [q_1, q_2]^T \in \mathbb{R}^2; \quad q_a = [q_3, q_4, q_5, q_6, q_7, q_8]^T \in \mathbb{R}^6$$

where q_u and q_a are un-actuated and actuated variables, respectively. The main idea in control design consists in the choice of particular reference trajectories for the actuated joints (q_a), to create a hybrid zero dynamic (HZD) for the dynamics of the un-actuated joints of the robot. A discrete-time event based feedback controller is then implemented to track the obtained trajectory and control the robot to recapture its stable cyclic walking after contact events. The reference trajectories are adapted after each impact.

Based on the method of virtual constraints [26], one holonomic constraint per actuator is considered in the form of an output that, when zeroed by a feedback controller, enforces the constraint. The constraint can be considered as

$$y = h(q) = q_a - h_d(\theta) \quad (13)$$

where θ is considered to be a quantity that is strictly monotonic (i.e., strictly increasing or decreasing) during the swing phase, and $h_d(\theta)$ is the desired evolution of the actuated variables. Roughly speaking, θ is used to replace time in parameterization of the trajectories. In a forward walking motion, if a virtual stance leg is defined by the line that connects the stance foot to the stance hip, then the angle of this virtual leg in the sagittal plane is monotonic (strictly increasing) because the z-coordinate of the hip increases monotonically. In this paper the length of the shank and the thigh are considered to be the same, and therefore the angle of the virtual leg is calculated as

$$\theta = -(q_2 + q_3/2) \quad (14)$$

The minus sign is used to make θ strictly increasing over a step. The output $y = h(q)$ depends only on the configuration variables, its relative degree is at least two. Differentiating the output twice and using Lie notation and state space model (Eq. 11) gives

$$\ddot{y} = L_f^2 h(q, \dot{q}) + L_g L_f h(q) u \quad (15)$$

where the decoupling matrix $L_g L_f h(q)$ is supposed to be permanently invertible and using equation 1 it is defined as follows

$$L_g L_f h(q) = \frac{\partial h(q)}{\partial q} M^{-1} S$$

A feedback controller to asymptotically drive the state of the robot to the constraint surface, is obtained by the input-output linearizing controller

$$u = u^* - \left(\frac{\partial h(q)}{\partial q} M^{-1} S \right)^{-1} \left(\frac{K_p}{\varepsilon^2} y + \frac{K_d}{\varepsilon} \dot{y} \right) \quad (16)$$

To zero the output y the required torque u^* can be computed as

$$u^* = \left(\frac{\partial h(q)}{\partial q} M^{-1} S \right)^{-1} \left(\frac{\partial^2 h_d(\theta)}{\partial \theta^2} \dot{\theta}^2 + \frac{\partial h(q)}{\partial q} M^{-1} (N(q, \dot{q}) \dot{q} + G(q)) \right) \quad (17)$$

If the feedback u applied to Eq. 15 results in

$$\ddot{y} + \frac{K_d}{\varepsilon} \dot{y} + \frac{K_p}{\varepsilon^2} y = 0 \quad (18)$$

Perfect tracking of the virtual constraints results in $q_a = h_d(\theta)$ and reduces the dimension of the dynamics. If we represent the vector of un-actuated joints as $q_u = [q_1, \theta]^T$ a linear relation exists between q , q_u , and q_a

$$q = \mathcal{T} \begin{bmatrix} q_u \\ q_a \end{bmatrix} \quad (19)$$

where $\mathcal{T} \in \mathbb{R}^{8 \times 8}$ is an invertible matrix. Then, Eq. (1) can be rewritten as

$$\begin{aligned} \mathcal{T}^T M(q) \mathcal{T} \begin{bmatrix} \ddot{q}_u \\ \ddot{q}_a \end{bmatrix} + \mathcal{T}^T (N(q, \dot{q}) \dot{q} + G(q)) \\ = \mathcal{T}^T S u = \begin{bmatrix} 0_{2 \times 6} \\ I_{6 \times 6} \end{bmatrix} u \end{aligned} \quad (20)$$

The dynamics of the un-actuated joints can be extracted from the first two lines of the above equation

$$M_{11}(q) \ddot{q}_u + M_{12}(q) \ddot{q}_a + N_1(q, \dot{q}) \dot{q} + \quad (21)$$

$$G_1(q) = 0_{2 \times 1}$$

where $M_{11} \in \mathbb{R}^{2 \times 2}$, $M_{12} \in \mathbb{R}^{2 \times 6}$, $N_1 \in \mathbb{R}^{2 \times 1}$ and $G_1 \in \mathbb{R}^{2 \times 1}$ are appropriate components of the coefficients of equation (20). Substituting the expressions of q_a , \dot{q}_a , and \ddot{q}_a corresponding to the virtual constraints, the swing phase zero dynamics of the single support phase obtained

$$\begin{aligned} M_{11}(q_u) \begin{bmatrix} \ddot{q}_u \\ \ddot{\theta} \end{bmatrix} + M_{12}(q_u) \left(\frac{\partial h_d(\theta)}{\partial \theta} \ddot{\theta} + \frac{\partial^2 h_d(\theta)}{\partial \theta^2} \dot{\theta}^2 \right) \\ + N_1(q_u, \dot{q}_u) + G_1(q_u) \\ = 0 \end{aligned} \quad (22)$$

This dynamic depends on the particular choice of the virtual constraint $y = q_a - h_d(\theta) = 0$. In the rest of this section, determination of $h_d(\theta)$ is summarized. $h_d(\theta)$ should be designed in a way that retrieves the cyclic motion under push and in the absence of the push results in a periodic walking motion.

Generation of virtual constraints is closely related to that of Chevallereau et al. [19, 20]. The problem of generation of the virtual constraints can be cast as a parameter optimization problem. To this end, a derivable continuous periodical parameterized function that allows to easily taking into account boundary conditions on the configuration and velocity at the beginning and end of a step should be defined. Bezier polynomials have such characteristics and they have a local control property like B-spline curves. Here, the virtual constraints are parameterized with Bezier polynomials of degree 3

$$h_d(\theta) = \sum_{k=0}^3 \alpha_k \frac{3!}{k!(3-k)!} s^k (1-s)^{3-k} \quad (23)$$

where α_k are coefficients of Bezier polynomials, $s = (\theta - \theta_i) / (\theta_f - \theta_i)$ is the normalized independent variable, θ_i and θ_f are the values of θ just before and just after the impact, respectively. Coefficients of Bezier polynomials must be determined so as to join initial configuration $(q_i)_a$ to final configuration $(q_f)_a$ and initial angular velocity $(\dot{q}_i)_a$ to final angular velocity $(\dot{q}_f)_a$ when θ varies from θ_i to θ_f . Therefore

$$\alpha_0 = h_d(\theta_i) = (q_i)_a \quad (24)$$

$$\begin{aligned}\alpha_1 &= (q_i)_a + \frac{\theta_f - \theta_i}{3} \frac{\partial h_d}{\partial \theta}(\theta_i) \\ &= (q_i)_a + \frac{\theta_f - \theta_i}{3} \frac{(\dot{q}_i)_a}{\dot{\theta}_i}\end{aligned}$$

$$\begin{aligned}\alpha_2 &= (q_f)_a - \frac{\theta_f - \theta_i}{3} \frac{\partial h_d}{\partial \theta}(\theta_f) = (q_f)_a \\ &\quad - \frac{\theta_f - \theta_i}{3} \frac{(\dot{q}_f)_a}{\dot{\theta}_f}\end{aligned}$$

$$\alpha_3 = h_d(\theta_f) = (q_f)_a$$

It should be mentioned that the evolution of the unactuated variables is obtained by integration of the dynamic subsystem (22).

A periodic walking orbit can be calculated by minimizing the energy consumption per step

$$J = \frac{1}{L} \int_0^\tau u^{*T} Q u^* dt \quad (25)$$

where τ is the walking period, Q is weighting matrix and L is the step length. The problem of optimization consisted of determining the initial and final configuration and velocity of the robot that could minimize the nonlinear objective function (Eq. (25)). To produce realistic values for optimization parameters the following constraints has been considered

- (a) θ is strictly increasing ($\dot{\theta} > 0$),
- (b) the swing foot is positioned above the ground ($x_{\text{swing}} > 0$),
- (c) a step size constraint,
- (d) a friction constraint,
- (e) the solution is periodic and symmetric with respect to the two legs.

When an impact with ground occurs, in the beginning of each step, the virtual constraints may not be satisfied. The virtual constraints are modified after events so that they are compatible with the initial state of the robot at the beginning of each step. So the new output for the feedback control design is

$$y_c = h(q, y_i, \dot{y}_i) = q_a - h_d(\theta) - h_c(\theta, y_i, \dot{y}_i) \quad (26)$$

This output consists of the previous output (Eq. (13)), and a correction term h_c that depends on Eq. (13) evaluated at the beginning of the step, specifically, $y_i = q_{a,i} - h_d(\theta_i)$ and $\dot{y}_i = \dot{q}_{a,i} - (\partial h_d(\theta)/\partial \theta)\dot{\theta}_i$, where the subscript i denotes the initial value for the current step. The values of y_i and \dot{y}_i are updated at the beginning of each step. The function h_c is taken as to be a three times continuously differentiable function of θ such that

$$\begin{cases} h_c(\theta_i, y_i, \dot{y}_i) = y_i \\ \frac{\partial h_c}{\partial \theta}(\theta_i) = \frac{\dot{y}_i}{\dot{\theta}_i} \\ h_c(\theta_i, y_i, \dot{y}_i) \equiv 0, \quad \frac{\theta_i + \theta_f}{2} \leq \theta \leq \theta_f. \end{cases} \quad (27)$$

If h_c considered as above, the output and its derivative are smoothly joined to the original virtual constraint in the middle of the step.

Event based ODE solver of MATLAB has been exploited to integrate the equations of motion. An event function locates the time when the height of swing leg (x_{swing}) passes through zero and stop integration. This automatically detects the contacts of the leg with ground and then impact map is used to obtain the new initial condition for next step. It should be noted that the stability of the walking under closed-loop control is usually evaluated numerically with the linearization of the restricted Poincaré map of the HZD [27, 28]. In this paper stability (convergence to the periodic motion) has been shown by simulations.

4. Results and discussion

4.1 Simulation results

The physical parameters of the biped model for the simulations are listed in Table 1. The aims of simulation scenarios presented here are to demonstrate the capability of the method for cyclic gait generation and push recovery under different kind of push disturbances. Several scenarios have been considered. First consider normal periodic walking with a perturbed initial condition. Figure 3 displays the phase portrait of the joints in the absence of disturbance. This is as an illustration of the behavior of the states of the robot. Straight lines show the impacts with the ground. It is seen that there is a periodic orbit for the joints which shows the periodic stability of the motion. The step time and the step length for this cyclic walking are $T = 0.245$ s, $L = 0.26$ m, respectively. The applied torques on the actuated joints during periodic walking cycles

are shown in Figure 4. Figure 5 Shows stick diagram of the biped motion in three views.

Table 1. Anthropometric parameters of the simulated model

Segment	Shank	Thigh	Torso
Length (m)	0.405	0.405	0.773
Mass (kg)	6.433	13.833	46.900
Center of mass position (m)	0.230	0.230	0.290

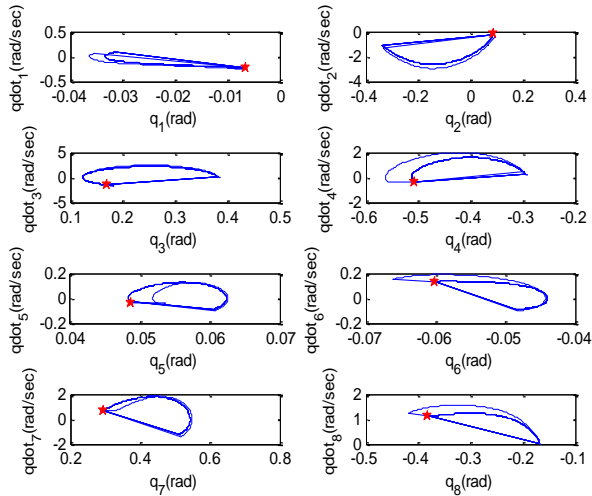


Fig. 3. Phase plane portraits of the joints for normal walking over eight steps. The star dots represent the initial state.

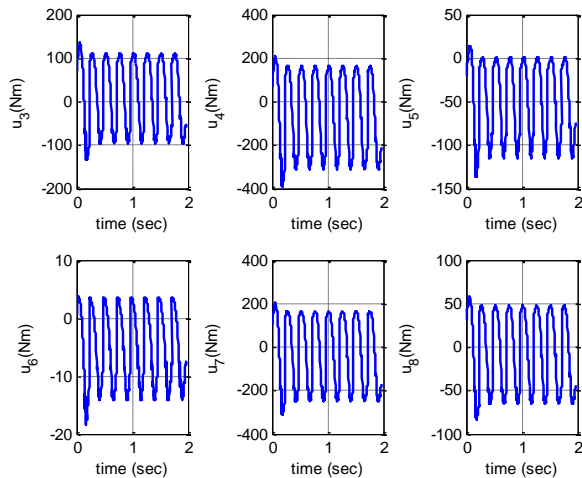


Fig. 4. The applied torques on the actuated joints during periodic walking cycles over eight steps.

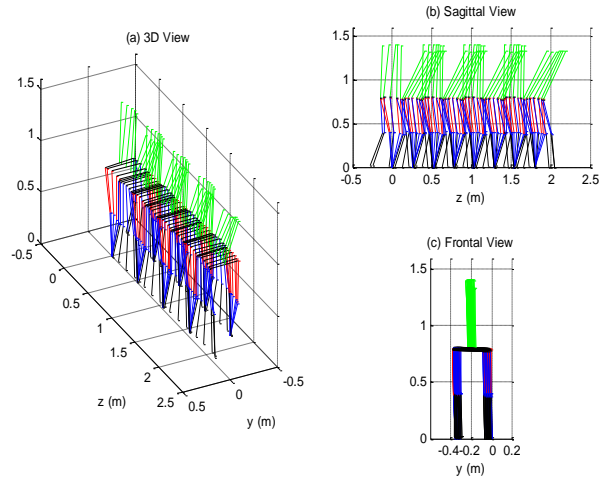


Fig. 5. Stick diagram of the walking.

The simulation results clearly show the convergence of the all trajectories (for both the controlled and uncontrolled variables) to an orbit. Now, consider a 0.5Ns forward push in the sagittal plane is applied at the early swing phase of the fourth step of walking. Figure 6 depicts the phase portrait of the joint variables after above mentioned push, where we note the convergence to a cycle after a deviation due to push. The phase portrait plots of the joint variables after applying 0.3Ns push in the early swing phase of the fourth step of walking in the frontal plane is depicted in Figure 7. The pushing force direction is from right to left when the left leg is supporting leg. The convergence to a periodic cycling is seen after a deviation due to push. Comparison of figure 6 and figure 7 shows that there are different evolutions of the states for all degrees of freedoms in the sagittal and frontal planes. For instance, for q_2 the deviation is more when the push occurs in sagittal plane in comparison with frontal case. Figure 8 shows the phase plane portraits of the joints for a push in both planes (0.5Ns forward push and 0.3Ns in the frontal plane from left to right) applying at the early swing phase of the fourth step.

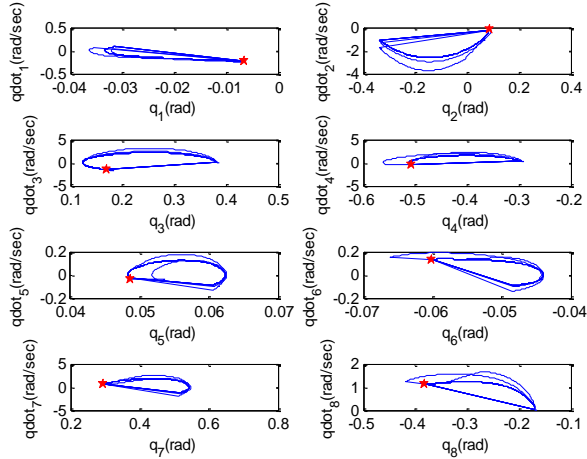


Fig. 6. Phase plane portraits of the joints for 0.5Ns forward push in the sagittal plane at the early swing phase of the fourth step of walking. The star dots represent the initial state.

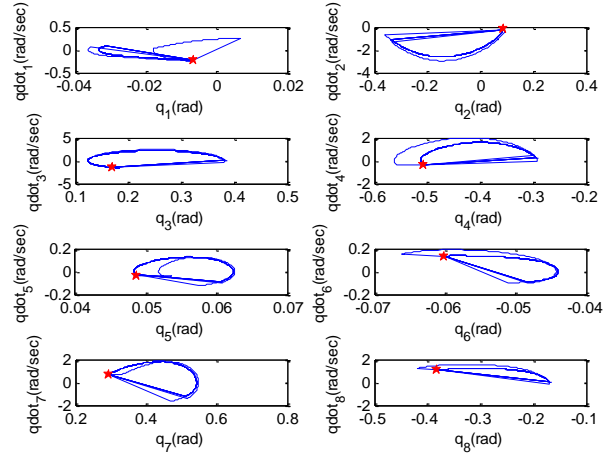


Fig. 7. Phase plane portraits of the joints for 0.3Ns push occurs in the frontal plane from right to left at the early swing phase of the fourth step of walking. The star dots represent the initial state.

Although, it is possible to use quantitative indexes [29] to show how robust the robot is, but we use a direct procedure to measure disturbance rejection abilities of the robot. The maximum pushes can be recovered in the sagittal and frontal planes at the early, mid and the late swing phase of the walking have been summarized in Figure 9 and 10, respectively. As seen, the capability of the biped for backward push recovery is more than with a forward push. This behavior can be explained as follows; the main critical moments for coming back to a stable motion after a push are the moments of applying and removing of the disturbance force. In the forward push after applying the force the controller tries to bring the model back to the stable posture but when the applied force zeroed (this is like a new disturbance in backward direction) the model lose the stability because the direction of reaction forces are against the walking direction. In the case of backward push, when the applied force removed (this is like a new disturbance in forward direction) the model can easily come back to a periodic walking cycle because the direction of reaction forces is same with walking direction.

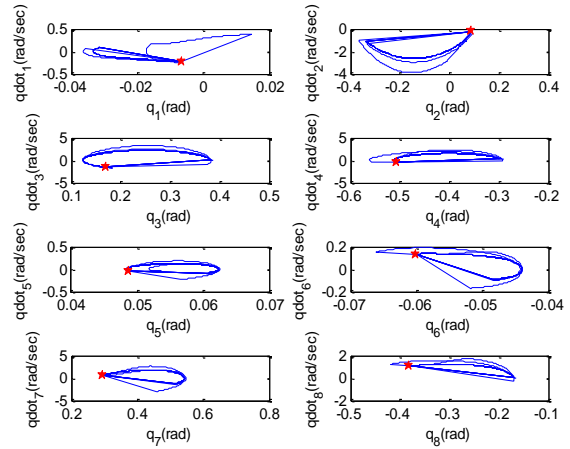


Fig. 8. Phase plane portraits of the joints for 0.5Ns forward push and 0.3Ns in frontal plane applied at the early swing phase of the fourth step of walking. The star dots represent the initial state.

Although, it is possible to use quantitative indexes [29] to show how robust the robot is, but we use a direct procedure to measure disturbance rejection abilities of the robot. The maximum pushes can be recovered in the sagittal and frontal planes at the early, mid and the late swing phase of the walking have been summarized in Figure 9 and 10, respectively. As seen, the capability of the biped for backward push recovery is more than with a forward push. This behavior can be explained as follows; the main critical moments for coming back to a stable motion after a push are the moments of applying and removing of the disturbance force. In the forward push after applying the force the controller

tries to bring the model back to the stable posture but when the applied force zeroed (this is like a new disturbance in backward direction) the model lose the stability because the direction of reaction forces are against the walking direction. In the case of backward push, when the applied force removed (this is like a new disturbance in forward direction) the model can easily come back to a periodic walking cycle because the direction of reaction forces is same with walking direction. The same argument is true for frontal plane disturbances (Figure 10) except for the late swing. At the late swing phase, when the left leg is supporting leg and the push direction is from left to right, the controller can recover from large amount of the push since when the push removed there are only two controlling torques against walking direction while the inertia of the model helps to continue stepping. At the late swing phase the model also is about to contact with the ground which produces angular momentum helping recovery.

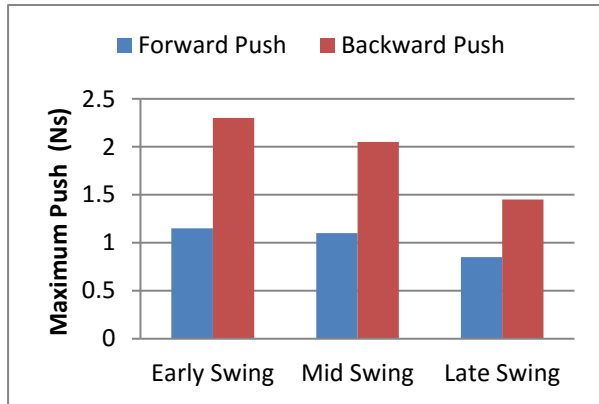


Fig. 9. Maximum sagittal pushes the method can recover at early, mid and late swing phase.



Fig. 10. Maximum frontal pushes the method can recover at early, mid and late swing phase. Left leg is supporting leg.

The range of maximum 3D pushes can be recovered by the model using the control strategy is depicted in Figure 11. These results have been obtained during the course of several simulations with different values of pushing forces in the both sagittal and frontal planes. Due to nonlinearity of equations, it is difficult to obtain an analytical relation for the range of disturbances that can be rejected by the model. The results of Figure 11 have been obtained for the push occurred at the early swing phase of the fourth step of the walking. As seen, when a combination of sagittal and frontal forces exerted on the model, the values of forces in sagittal and frontal directions can be exceed the values obtained for only in one direction. However, the value of maximum pushes that can be recovered in our method even with high gain controller is not much in comparison with ZMP based fully actuated models (e.g. see ref. (13) in which as an example their model can be recovered from 20Ns push). Success of our control law in rejection of higher magnitude pushes needs online redesigning of the virtual constraints for actuated joints after applying the push which is computationally expensive.

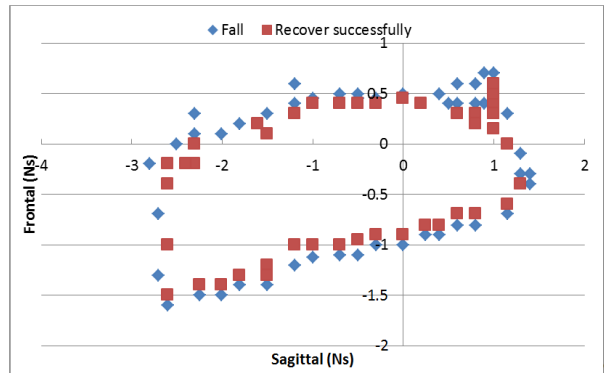


Fig. 11. The range of disturbing pushes that can be recovered by the method

4.2 Robustness against parameters uncertainty

In order to evaluate the robustness of the controller, two kind of parameter uncertainties are considered. First, an uncertainty of 15% for the nominal values of the inertias of the segments is considered. Figure 12 displays the comparison of the phase portraits for nominal and uncertain simulations. It is seen that there is a new periodic orbit for the joints which shows the stability of the motion with uncertainties. Second, an uncertainty of 10% on the mass of the torso is considered. Figure 13 shows the convergence to a new stable cyclic trajectory for the all joints of the uncertain system.

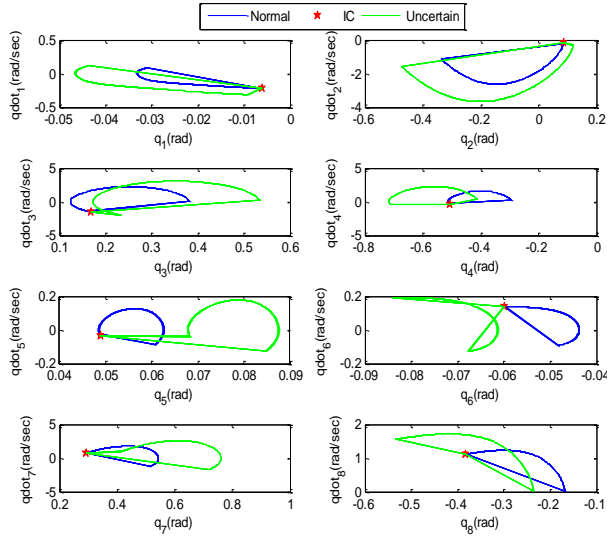


Fig. 12. Phase plane portraits of the joints. The star dots represent the initial condition (IC).

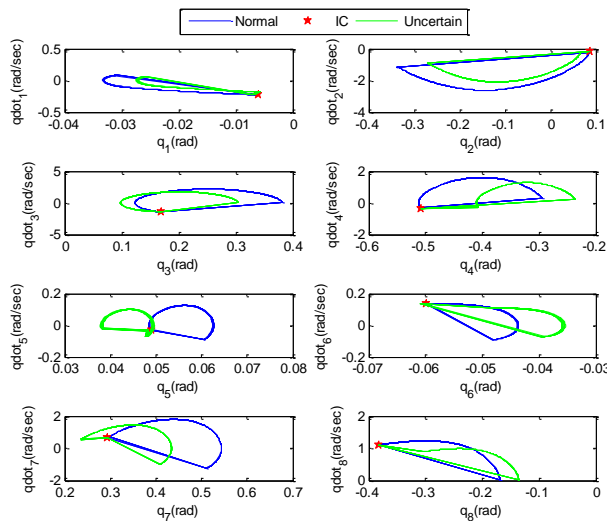


Fig. 13. Phase plane portraits of the joints. The star dots represent the initial condition (IC).

4.3 Qualitative comparison of results with strategies observed in human

Review of literature shows that most of the experimental work done by researchers are on the upright standing push recovery. But, there are few useful experimental results for human push recovery during walking [30-32]. Inspired by biomechanical and biological studies, some researchers have shown that the hip and ankle joints play an important role in rapid stepping to prevent falling during walking [33]. The first inspiration, hip strategy, is to generate a torque at the hip joint to compensate the angular acceleration induced by external forces. The second one, ankle

strategy is to propel the leg by creating large torques at ankle joint. Researchers have also introduced another strategy for mid-swing disturbances which is called knee strategy. Knee strategy functions in a way of holding and adjusting the stiffness at knee joint in the way that it can support the upper extremity.

In accordance with aforementioned strategies, some other researchers (e.g. [34]) have also reported that the more frequent strategies that are used by real subjects during perturbed swing phase of walking are

- (i). Elevating strategy which consists of elevation of the swing leg to overtake the obstacle. The step is lengthened (longer step time),
- (ii). Lowering strategy consists of bringing the foot to the ground as quickly as possible. The step lengths and time are reduced,
- (iii). Delayed lowering strategy could be understood as a failed elevating strategy in which the subject first tries an elevating strategy and then switches to a lowering one.

It should be noted that, human being reactions can be affected by neurological (e.g. muscular activation delay), psychological (e.g. fear of falling) and mechanical limitations (maximum torque and joint ranges of motion). For a biped model only the mechanical limitations make sense.

In all the simulations have been done for the current work, the delayed lowering strategy never were seen. For forward push the reaction of the model is like lowering strategy and the step time is reduced while the step speed is relatively increased. For backward push elevating strategy is used by the model to come back to periodic walking and the step time is increased while step speed is reduced. It should be noted that the model of this work, like all the other models based on conventional mechanics and controls, has inherent limitations (e.g. no actuation on the ankle joint). But, even whit this model it is possible to characterize obtained results in terms of movement strategies observed in the human after push.

5. Conclusions

In this paper an inverse biomimetic approach has been implemented to reproduce human reactions under pushing disturbance during walking. Generally, the main purpose of this work was to improve the compatibility and transferability of findings between roboticists and biologists. The results showed the ability of HZD feedback control method to reproduce human like movements for push recovery of an under-actuated 3D biped model when walking on a flat surface. This approach is based on the consideration of holonomic constraints on the configuration variables of the robot. These constraints are then used to construct

outputs of the system and when imposed by event-based feedback controller cause the robot to move in a stable manner. A constrained trajectory optimization, with initial and final configurations as the design parameters, is run offline to obtain optimum configuration of the robot in the end of the swing phase of walking. The outputs of system (reference trajectory of controller) are adjusted in the end of each contact with the ground to be compatible with the initial state of the robot at the beginning of next step. The results of our study showed the convergence of the all trajectories to a cyclic motion after push occurring in the sagittal and frontal plane and also in the both directions simultaneously. The results clearly showed that the ability of model in backward push recovery is more than forward push and the capability in tackling frontal pushes depends on which leg is supporting leg and also the direction of the pushing force. The amount of pushing disturbances can be rejected in the early swing phase is more than mid swing phase and it is also more than the late swing phase. It has also seen that the simulated results can be characterized in terms of some strategies observed in human being movements against perturbations. However, altogether the results showed that although the amount of the disturbance which can be rejected with this under-actuated model is not much but the motions obtained are natural and human like. We believe that adding appropriate learning algorithms will effectively increase the maximum push recovery capability (there is similar fact in biology, compare push recovery capability of the professional athletes and non-athletes persons or kids and adult persons).

In a future work, the control method will be extended to a robot model with higher degrees of freedom. Push recovery experiments on human will be done using motion capture systems. Parameters of the method then will be modified to obtain results which are mostly close to the experiments. It will be the subject of future work to design robust and adaptive controllers to overcome uncertainties. The quality of recovery (energy consumption) will also be considered.

References

1. A. Seyfarth, S. Grimmer, D. F. B. Haufle, K.T Kalveram, Can Robots Help to Understand Human Locomotion? *Automatisierungstechnik*, **60** (11) (2012) 653-660.
2. K. T. Kalveram, A. Seyfarth, Inverse biomimetics: How robots can help to verify concepts concerning sensorimotor control of human arm and leg movements, *Journal of Physiology-Paris*, **103** (3-5) (2009) 232-243.
3. T. Buschmann, A. Ewald, A. V. Twickel, and A. Büschges, Controlling legs for locomotion-insights from robotics and neurobiology, *Bioinspir. Biomim.* **10** (2015)1-38.
4. J. Rummel, Y. Blum, and A. Seyfarth, Robust and efficient walking with spring-like legs, *Bioinspir. Biomim.*, **5** (2010) 1-13
5. F. Boyer, and M. Porez, Multibody system dynamics for bio-inspired locomotion: from geometric structures to computational aspects, *Bioinspir. Biomim.* **10** (2015) 1-21.
6. J. Y. Jun, and J. E. Clark, Characterization of running with compliant curved legs, *Bioinspir. Biomim.* **10** (2015) 1-18
7. B. Stephens, *Push recovery control for force-controlled humanoid robots*, PhD thesis, Carnegie Mellon University, USA, 2011.
8. J. Pratt, J. Carff, S. Drakunov, and A.Goswami, Capture Point: A Step toward Humanoid Push Recovery, in: *6th IEEE-RAS International Conference on Humanoid Robots*, Genova, Italy, (2006) pp. 200 – 207
9. S. K. Yun, and A. Goswami, Momentum-Based Reactive Stepping Controller on Level and Non-level Ground for Humanoid Robot Push Recovery, *IROS 2011*, San Francisco, CA, September 2011.
10. B. Miripour Fard, A. Bagheri, A. S. Khoskbijari, Receding Horizon Based Control of Disturbed Upright Balance with Consideration of Foot Tilting, *IJE TRANSACTIONS A: Basics*, **26** (10) (2013) 1243-1254.
11. Y. J. Kim, J.Y. Lee, and J. J. Lee, A Torso-Moving Balance Control Strategy for a Walking Biped Robot Subject to External Continuous Forces, *Int. J. Humanoid. Robotics.* **12** (01) (2015).
12. Y. J. Kim, J.Y. Lee, and J. J. Lee, A Balance Control Strategy for a Walking Biped Robot under Unknown Lateral External Force using a Genetic Algorithm, *Int. J. Humanoid. Robotics.* **12** (02) (2015) 1-37
13. A. H. Adiwahono, C. M. Chew, W. Huang, and Y. Zheng, Push recovery controller for bipedal robot walking" In: *IEEE/ASME International Conference on Advanced Intelligent Mechatronics*, Singapore, (2009) pp.162-167.
14. A. H. Adiwahono, C. M. Chew, W. Huang and V. H. Dau, Humanoid robot push recovery through walking phase modification. In: *IEEE Conference on Robotics Automation and Mechatronics (RAM)*, (2010) pp. 569-574.
15. A. H. Adiwahono, C. M. Chew, and B. Liu, Push Recovery through Walking Phase Modification for Bipedal Locomotion, *Int. J. Human. Robot.* **10** (03) (2013) 1-30.
16. J. Urata, K. Nshiwaki, Y. Nakanishi, et al., Online decision of foot placement using singular LQ preview regulation, In: *2011 IEEE/RAS International Conference on Humanoid Robots*, Bled, Slovenia, (2011) pp.13-18.
17. T. Wang, Ch. Chevallereau and C. F. Rengifo, Walking and steering control for a 3D biped robot considering ground contact and stability, *Robotics and Autonomous Systems*; **60** (2012) 962-977.
18. B. Miripour Fard, A. Bagheri and N. Nariman-zadeh, Limit cycle walker push recovery based on a receding horizon control scheme, *Proc IMechE Part I: J Systems and Control Engineering*; **226**(7) (2012) 914-926.
19. Ch. Chevallereau, J. W. Grizzle and Ch. L. Shih, Asymptotically stable walking of a five-link underactuated 3-D bipedal robot, *IEEE Trans Robot*; **25**(1) (2009) 37-50.

- 20 Ch. Chevallereau, J. W. Grizzle and Ch. L. Shih, Steering of a 3D bipedal robot with an underactuated ankle, In: *2010 IEEE/RSJ International Conference on Intelligent Robots and Systems*, Taipei, Taiwan, (2010) pp.1242-1247.
- 21 G. Song and M. Zefran, Underactuated dynamic three-dimensional bipedal walking, In: *2006 IEEE International Conference on Robotics and Automation*, Orlando, FL, (2006) pp. 854-859.
- 22 D. Tlalolini, Ch. Chevallereau, and Y. Aoustin, Human-like walking: optimal motion of a bipedal robot with toe-rotation motion, *IEEE/ASME Transactions on Mechatronics*, **16**(2) (2011) 310-320.
23. J. J. Craig, *Introduction to Robotics Mechanics and Control*, 2th edn. (Addison- Wesley, USA, 1989), pp.196-205.
24. D. Tlalolini, Y. Aoustin and Ch. Chevallereau, Design of a walking cyclic gait with single support phases and impacts for the locomotor system of a thirteen-link 3D biped using the parametric optimization, *Multibody Syst Dyn*; **23** (2010) 33-56.
25. W. Khalil, and J. Kleinfinger, A new geometric notation for open and closed loop robots, In: *IEEE Conference on Robotics and Automation*, (1985) pp.1174-1180.
26. ER. Westervelt, J. W. Grizzle, Ch. Chevallereau, et al., *Feedback control of dynamic bipedal robot locomotion*, (London: Taylor and Francis/CRC, 2007).
27. B. Morris and J. W. Grizzle, A restricted Poincaré map for determining exponentially stable periodic orbits in systems with impulse effects: Application to bipedal robots,

- In: *2005 IEEE Conference on Decision and Control*, Seville, Spain, (2005) pp. 4199-4206.
28. B. Morris and J. W. Grizzle, Hybrid invariant manifolds in systems with impulse effects with application to periodic locomotion in bipedal robots, *IEEE Transactions on Automatic Control*, **54**(8) (2009) 1751-1764.
29. D.G.E. Hobbelen, and M. Wisse, A disturbance rejection measure for limit cycle walkers: the gait sensitive norm, *IEEE Trans. on Robotics*, **23**(6) (2007) 1213-1224.
30. V. B. Semwal, S. A. Katiyar, R. Chakraborty, G. C. Nandi, Biologically-inspired push recovery capable bipedal locomotion modeling through hybrid automata, *Robotics and Autonomous Systems* **70** (2015) 181-190.
31. V. B. Semwal, and G. C. Nandi, Toward Developing a Computational Model for Bipedal Push Recovery—A Brief, *IEEE Sensors Journal*, **15**(4) (2015) 2021-2022.
32. V. B. Semwal, A. Bhushan, and G. C. Nandi, Study of humanoid push recovery based on experiments, in: *Proceeding of IEEE International Conference on CARE*, (2013), pp. 1-6.
33. Z. Jie, S. Schutz, K. Berns, Biologically motivated push recovery strategies for a 3D bipedal robot walking in complex environments, in: *2013 IEEE International Conference on Robotics and Biomimetics, (ROBIO)*, Shenzhen, China, 2013, pp.1258-1263.
34. A. F. Cordero, HJFM. Koopman and FCT. Helm, Mechanical model of the recovery from stumbling, *Biological Cybernetics*, **91**(2004) 212-220.

Appendix A. Dynamic Equations based on NE recursive method

Suppose the robot is composed of $n+1$ links, link (0) is the fixed base, while link (n) is the terminal link. Joint (j) connects link (j -1) and link (j). Let

R_j the fixed frame with respect to link (j),
 z_j the axis of joint (j),
 x_j the common perpendicular of z_j and z_{j+1} (Figure A1).

The following parameters are required to define the frame (R_j) with respect to frame (R_{j-1})

α_j : angle between z_{j-1} and z_j about x_{j-1} ,

d_j : distance between o_{j-1} and z_j ,

r_j : distance between o_j and x_{j-1} ,

θ_j : angle between x_{j-1} and x_j about z_j .

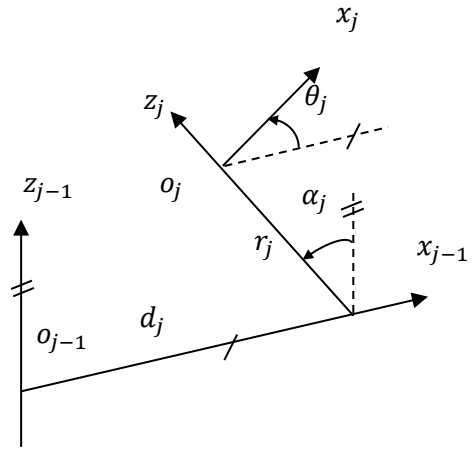


Figure A1. Notation for two adjacent joints.

The above parameters for the model presented in Figure 1 are given in Table A1. It should be noted that for the biped model $n=8$ and $q_9 = 0$. It is considered that the frame (R_0), is fixed to the tip of the stance foot and the frame (R_9) is fixed to the tip of the swing foot.

Table A1. Modified D-H parameters of the model

Joint	α_j	θ_j	r_j	d_j
1	0	q_1	0	0
2	$\pi/2$	q_2	0	0
3	0	q_3	0	d_3
4	0	q_4	r_4	d_4
5	$-\pi/2$	$(q_5 - \pi/2)$	0	0
6	0	$(q_6 - \pi/2)$	0	d_6
7	$-\pi/2$	q_7	0	0
8	0	q_8	r_8	d_8
9	0	$q_9 = 0$	$r_9 = 0$	d_9

The transformation matrix is then equal to

$${}^{j-1}T_j = \begin{bmatrix} \cos \theta_j & -\sin \theta_j & 0 & d_j \\ \cos \alpha_j \sin \theta_j & \cos \alpha_j \cos \theta_j & -\sin \alpha_j & -r_j \sin \alpha_j \\ \sin \alpha_j \sin \theta_j & \sin \alpha_j \cos \theta_j & \cos \alpha_j & r_j \cos \alpha_j \\ 0 & 0 & 0 & 1 \end{bmatrix}$$

The geometric model of the robot will be obtained by the successive multiplication of the transformation matrices.

$${}^0T_n = {}^0T_1 {}^1T_2 \dots {}^{n-1}T_n$$

NE method is based on two recursive calculations; outward and inward calculations. The outward calculation, from the base (stance foot) to the terminal link (swing foot) determines the velocity, the accelerations, and the total forces and moments on each link. Then the inward calculations, from swing foot to stance foot, gives the joint torques and reaction forces using equation of equilibrium of each link successively.

Outward iterations $j = 1 \rightarrow 9$

During single support phase the contact point of the robot remains on the ground, the initial conditions are

$${}^0\omega_0 = 0_{6 \times 1}, \quad {}^0\dot{\omega}_0 = 0_{6 \times 1} \quad \text{and} \quad {}^0\dot{V}_0 = -[g \quad 0 \quad 0]^t$$

Angular velocity of link j (${}^j\omega_j$) and the linear velocity of the origin o_j of R_j (jV_j) are obtained as

$${}^j\omega_j = {}^jR_{j-1} {}^{j-1}\omega_{j-1} + \dot{q}_j {}^jZ_j \quad (\text{A.1})$$

$${}^jV_j = {}^jR_{j-1} ({}^{j-1}V_{j-1} + {}^{j-1}\hat{\omega}_{j-1} \times {}^{j-1}P_j) \quad (\text{A.2})$$

in which ${}^jR_{j-1}$ is the orientation matrix of the frame R_{j-1} in the frame R_j and Z_j is a unit vector along the Z axis, ${}^{j-1}P_j$ is the vector expressing the origin of frame R_j in the frame R_{j-1} . The angular acceleration of link j and the linear acceleration of the origin o_j of R_j are

$${}^j\dot{\omega}_j = {}^jR_{j-1} {}^{j-1}\dot{\omega}_{j-1} + {}^jR_{j-1} {}^{j-1}\omega_{j-1} \dot{q}_j {}^jZ_j + \ddot{q}_j {}^jZ_j \quad (\text{A.3})$$

$${}^j\dot{V}_j = {}^jR_{j-1} ({}^{j-1}\dot{\omega}_{j-1} \times {}^{j-1}P_j + {}^{j-1}\omega_{j-1} \times ({}^{j-1}\omega_{j-1} \times {}^{j-1}P_j) + {}^{j-1}\dot{V}_{j-1}) \quad (\text{A.4})$$

The linear acceleration of mass center of segment j relative to the frame j is

$${}^j\dot{V}_{c_j} = {}^j\dot{\omega}_j \times {}^jP_{c_j} + {}^j\omega_j \times ({}^j\omega_j \times {}^jP_{c_j}) + {}^{j-1}\dot{V}_{c_{j-1}} \quad (\text{A.5})$$

where ${}^jP_{c_j}$ is the position vector of mass center of the link j relative to the frame j . Inertia force (jF_j) and inertia torque (jN_j) are obtained as follow

$${}^jF_j = M_j {}^j\dot{V}_{c_j} \quad (\text{A.6})$$

$${}^jN_j = {}^{cj}J_j {}^j\dot{\omega}_j + {}^j\omega_j \times {}^{cj}J_j \times {}^j\omega_j \quad (\text{A.7})$$

in which ${}^{cj}J_j$ is inertia tensor of the link j with respect to the frame cj which is located in the center of mass of the link j .

Inward iterations $j = 9 \rightarrow 1$

The force exerted on segment j by segment $j-1$ and torque exerted on segment j by segment $j-1$ are obtained

$${}^j f_j = {}^jR_{j+1} {}^{j+1}f_{j+1} + {}^jF_j \quad (\text{A.8})$$

$${}^j n_j = {}^jN_j + {}^jR_{j+1} {}^{j+1}n_{j+1} + {}^jP_{c_j} \times {}^jF_j + {}^jP_{j+1} \times {}^jR_{j+1} {}^j f_{j+1} \quad (\text{A.9})$$

The torque u_j (components of u in Eq. (1)) is then obtained by projecting ${}^j n_j$ along the joint axis jZ_j :

$$u_j = {}^j n_j \cdot {}^jZ_j \quad (\text{A.10})$$

It should be noted that in the single support phase ${}^9f_9 = 0$ and ${}^9n_9 = 0$.

Biography



Behnam Miripour Fard received his BSc degree in Mechanical Engineering from the University of Guilan, Rasht, Iran in 2005, his MSc degree in Mechanical Engineering from the Bu-Ali Sina University, Hamedan, Iran, in 2008, and his Ph.D. degree in Mechanical

Engineering from the University of Guilan, Rasht, Iran in 2013. From Apr. 2012 to Oct. 2012, he was a visiting PhD Student at Robotics Institute of Carnegie Mellon University, Pittsburgh, PA, USA. He is currently an Assistant Professor and the head of the Robotics Engineering Department of the Hamedan University of Technology, Hamedan, Iran. Dr. Miripour Fard is the author/coauthor of over 40 technical publications, proceedings, editorials and books. He has been a Member of Iranian Elite Foundation and Inventors Association since 2007. His research interests include; Dynamical modeling of Mechanical systems, Path Planning and Control of Humanoid Biped Robots, Limit Cycle Walking, Disturbance Rejection of Legged Locomotion, Predictive Dynamics and Bio-mimetic approaches in robotics.



Ahmad Bagheri received his BSc degree in Mechanical Engineering from the University of Mashhad, Mashhad, Iran in 1989, his MSc degree from the University of Tarbiat Modares, Tehran, Iran in 1993, and his Ph.D. degree in Mechatronics from Czech Technical

University in Prague, Prague, the Czech Republic, in 1997. He is currently serving as a Full Professor of Mechanical Engineering Department of The University of Guilan, Rasht, Iran. His research interests include mechatronics, biped locomotion, robot modeling and control, and industrial robotics.



Nader Nariman-zadeh received his MSc (Eng.) degree in mechanical engineering from Tehran University, Iran, in 1986 and the PhD degree in intelligent control from Salford University, England, in 1996. He then joined the Department of Industrial Manufacturing and Systems

Engineering of the University of Hong Kong for his postdoctoral period. He is a professor in the Department of Mechanical Engineering of the University of Guilan and Intelligent-based Experimental Mechanics Center of Excellence, School of Mechanical Engineering, Faculty of Engineering, University of Tehran. He was also a visiting associate professor at the University of Birmingham, UK, 2002–2003. He has served as the head of Mechanical Engineering Department, dean of faculty of Engineering, deputy of chancellor in research of the University of Guilan. His research interests are intelligent control and modelling using evolutionary algorithms, fuzzy logic, and GMDH-type neural networks, multi-objective optimization in modelling and control, robust and reliability-based design and optimization using evolutionary algorithms.